



Simulation of a large methanol-to-olefins fluidized bed reactor with consideration of coke distribution



Jingyuan Zhang^{a,b,c}, Bona Lu^{a,b,*}, Feiguo Chen^a, Hua Li^d, Mao Ye^d, Wei Wang^{a,b}

^a State Key Laboratory of Multiphase Complex Systems, Institute of Process Engineering, Chinese Academy of Sciences, Beijing 100190, China

^b Sino-Danish College, University of Chinese Academy of Sciences, Beijing 100049, China

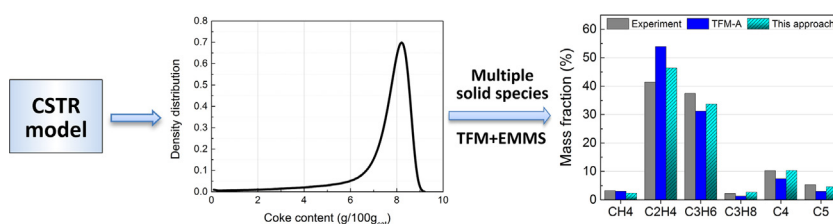
^c Department of Energy and Process Engineering, Norwegian University of Science and Technology, Kolbjørn Hejes vei 1b, 7491 Trondheim, Norway

^d National Engineering Laboratory for MTO, Dalian Institute of Chemical Physics, Chinese Academy of Sciences, Dalian 116023, China

HIGHLIGHTS

- A CSTR model considering the content distribution is established.
- The solid phase is treated as a mixture of a series of solid species with different coke contents.
- This approach requires 36% more computation time compared with the previous study.
- The predictions of reaction quantities are improved using this approach.

GRAPHICAL ABSTRACT



ARTICLE INFO

Article history:

Received 5 January 2018

Received in revised form 25 May 2018

Accepted 28 May 2018

Available online 30 May 2018

Keywords:

Methanol-to-olefins

Coke distribution

Fluidized bed

Simulation

EMMS

ABSTRACT

In the methanol-to-olefins (MTO) process, coke deposition is closely related to the selectivity of light olefins. Previous simulations of different-sized MTO reactors using two-fluid model (TFM) combined with the EMMS (energy minimization multi-scale)-based drag well predict the hydrodynamic behaviors but poorly predict the product distribution of large reactors due to the unreasonable prediction in coke distribution. In this study, the TFM integrated with the EMMS-based drag is still employed, but the solid phase is treated as a mixture of a series of species with different coke contents. Because the coke content depends on the age of catalyst particles inside the reactor, a continuous stirred tank reactor (CSTR) model mimicking turbulent fluidization while considering the age distribution of catalysts is established to predict the initial coke distribution for speeding up simulation. Compared with the previous simulation without consideration of coke distribution, this approach increases the computational time by a factor of 36% and shows no influence on hydrodynamic predictions, but the reaction quantities such as methanol conversion, mass fractions of gaseous products and selectivity of light olefins, are better predicted.

© 2018 Elsevier Ltd. All rights reserved.

1. Introduction

The methanol-to-olefins (MTO) process creates a new route to produce light olefins such as ethylene and propylene (Tian et al., 2015). Methanol can be readily obtained from oil and non-oil feedstock including coal and natural gas (Amghizar et al.,

2017), thus diversifying the production of light olefins and making the MTO process attractive, especially in China. At present, there are several successful MTO techniques brought into stream, such as the processes developed from Dalian Institute of Chemical Physics (DICP), SINOPEC, UOP and ExxonMobil (Keil, 1999, Chen et al., 2005, Tian et al., 2015, Ye et al., 2015), respectively. In 2010, the World's first commercial unit (1800 kt/a methanol feedstock) using the DICP's MTO (DMTO) technique was successfully operated in Baotou plant of Shenhua group (Tian et al., 2015). The MTO process is expected to be the primary route for producing light olefins in the future.

* Corresponding author at: State Key Laboratory of Multiphase Complex Systems, Institute of Process Engineering, Chinese Academy of Sciences, Beijing 100190, China.

E-mail address: bnlu@ipe.ac.cn (B. Lu).

Nomenclature

C	concentration, mol/L
C_{D0}	standard drag coefficient for an individual particle
d_p	particle diameter, m
g	gravitational acceleration, kg/m ² /s
G_s	mass flow rates of the recycled catalysts, g/s
H_D	heterogeneity index
k_i	reaction rate constant, L/(g _{cat} ·s)
M	molecular weight, g/mol
p	pressure, Pa
Q	volumetric flow rate of gas phase, L/s
R_i	reaction rate, g/(g _{cat} ·s)
u	real velocity, m/s
v	stoichiometric number
w_c	coke content, g/100g _{cat}
Y	mass fraction

Greek letters

β	drag coefficient with structure in a control volume, kg/(m ³ ·s)
Γ	interphase mass transfer, kg/m ² /s
ε	volume fraction
μ	viscosity, Pa·s
ρ	density, kg/m ³
τ	stress tensor, N/m ²
φ	deactivation function
η	methanol conversion

Subscripts

g	gas phase
s	solid phase
i, j	lump in reaction kinetics/interval

The design of the MTO process originates from the concepts of modern fluid catalytic cracking (FCC) units, but it has distinctive characteristics (Ye et al., 2015), taking the DMTO process as an example: first, the SAPO-34 catalysts used in MTO have much smaller pores (<2 nm) than the zeolite Y catalysts in FCC, so the coke deposition which could decrease the pore size shows a close relation to the selectivity of ethylene (Li et al., 2016); second, because long residence time of catalysts (on the order of tens of minutes) is required to achieve the optimum coke content, dense fluidized bed such as a turbulent bed is preferred in the MTO process while a riser reactor is often used in modern FCC units. Hence optimization of the current MTO technology calls for further fundamental research to fully understand the hydrodynamics and reaction behaviors in the reactor.

In early research, classic reactor models were widely applied to describe the simplified hydrodynamics (Bos et al., 1995, Schoenfelder et al., 1996, Soundararajan et al., 2001, Alwahabi and Froment, 2004, Kaarsholm et al., 2010). Alwahabi and Froment (2004) coupled chemical kinetics with three reactor models (the multi-tubular quasi-isothermal reactor model, multi-bed adiabatic reactor model and bubbling fluidized bed model) separately to search for the optimal reactor type. Soundararajan et al. (2001) employed a core-annulus two-phase model with a lumped kinetic model to investigate the reaction performance. Generally, reactor models have been found to be suitable for predicting mean quantities and steady state behaviors. In recent years, the rapidly developing Computational Fluid Dynamics (CFD) has been extensively used to investigate complex hydrodynamics and reactions in fluidized beds. Chang et al. (2013) applied the TFM with a lumped kinetic model to simulate a small fast bed reactor and analyzed the effects of operating conditions including gas velocity, solid circulation rate, temperature and coke content. Zhuang et al. (2014) employed the discrete particle model (DPM) and the kinetic model of Bos et al. (1995) to simulate a very small two-dimensional (2D) reactor and obtained detailed hydrodynamic quantities. Zhao et al. (2013) used the TFM and the EMMS/bubbling drag to simulate a demo-scale DMTO turbulent reactor and found a good prediction in pressure distribution. Zhu et al. (2016) re-simulated this turbulent reactor by changing the drag model and studied the effects of reaction kinetic models on the results. These studies are more focused on model validation.

To further develop and optimize the MTO process, DICP cooperated with Institute of Process Engineering (IPE) to conduct a series of CFD simulations of DMTO reactors ranging from the micro to commercial scale. Simulations of different-sized reactors pose a big challenge to CFD modeling in the following aspects: (i) because

DMTO reactors are operated at dense fluidization with long residence time, even simulations using coarse-grid resolution require formidable computational cost. Hence speeding up the simulation is very necessary; (ii) because the flow regime changes from the bubbling fluidization to turbulent fluidization on upscaling the DMTO reactor (Tian et al., 2015, Lu et al., 2017), these changes should be taken into account in drag modeling which is a key factor of CFD simulations of fluidized beds (Li & Kwauk, 2003, Yang et al., 2003, Wang & Li, 2007, Stroh et al., 2016, Kraft et al., 2017, Luna et al., 2017); (iii) the chemical kinetic model was obtained from experiments on the micro-scale reactor (Ying et al., 2015, Yuan et al., 2017), so the applicability of this model to simulations of larger reactors having different hydrodynamic behaviors needs to be further investigated. Lu and coworkers conducted a series of researches (Lu et al., 2016, 2017, Luo et al., 2017): first, a continuous-stirred tank reactor (CSTR) model was established to predict mean coke content. It was found that using the mean coke content as the initial value, the reactive simulation of a pilot-scale bubbling fluidized bed can quickly reach the pseudo-steady state (Lu et al., 2016); second, the EMMS/bubbling model which is more suitable for bubbling fluidization was extended to a two-step version whose heterogeneity index depends on both voidage and slip velocity. The relevant simulations show a weak dependence on grid size and better predictions for the turbulent fluidized bed (Luo et al., 2017); third, a series of simulations of different-sized DMTO reactors were conducted by using the TFM and the two-step drag model in conjunction with the lumped kinetics from the experiments on the micro-scale reactor. It was found that hydrodynamic behaviors in these MTO reactors are successfully captured, but there is a big discrepancy between reaction quantities from simulations and experimental data for large reactors (Lu et al., 2017).

Ye et al. (2015) reported that there is a wide distribution of coke content in large MTO fluidized bed reactors because of the significant circulation of catalysts and the formation of meso-scale structures, whereas our previous work (Lu et al., 2017) predicted uniform coke distribution in the reaction zones of large reactors. Lu et al. (2017) pointed out that the coke content depends closely on the residence time of catalysts, while the TFM simulation averages different coke contents in a computational cell and is thus unable to capture the realistic change of coke content.

In this study, we aim to improve the reactive simulations of large MTO reactors by differentiating catalysts with different coke contents under the TFM framework. The basic governing equations and chemical kinetic model are first presented. Then a CSTR model is extended by considering the age distribution of catalysts to

estimate the distribution of coke content which is then set as the initial condition of CFD simulations. The parameter analysis with emphasis on solid species number is conducted, followed by a comparison of experimental data and simulation results of hydrodynamics and product distribution. Finally, conclusions and future work are provided.

2. Experimental setup

The geometry of the demo-scale DMTO reactor with a methanol feed of 16 kt/a is shown in Fig. 1. The reaction zone is 4.0 m high and 1.25 m in I.D., which is operated in turbulent fluidization and equipped with a water cooling jacket to maintain relatively constant temperature (around 773 K). The gas distributor at the bottom of the reaction zone has small nozzles pointing upward and thus allows the gas stream to enter the reaction zone at high velocity. The upper enlarged region with a height of 2.62 m is the freeboard/disengaging zone. Below the distributor is the stripper for discharging spent catalysts. The catalyst inlet is located in the center of the reaction zone has the diameter of 0.1 m. The main stream of reactants (methanol and steam) flows into the reaction zone below the distributor with a total flow rate of 2642 kg/h (2032 kg/h for methanol and 610 kg/h for H₂O). Fresh catalysts are fed into the reactor zone with a flow rate of 351 kg/h. A series of reactions take place once the reactants contact with catalysts. The coke is then generated and affects the reaction rate. The

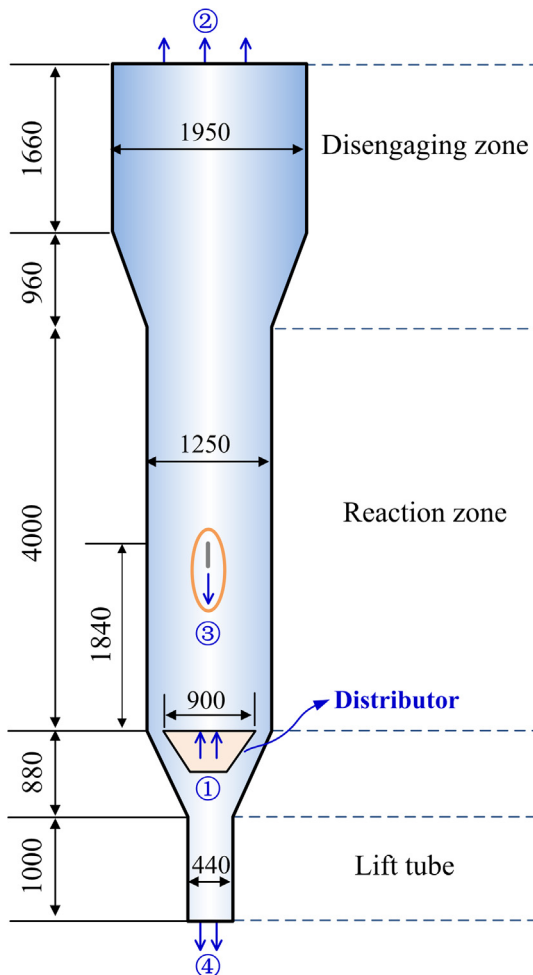


Fig. 1. The schematic diagram of a demo-scale DMTO fluidized bed: ① inlet for methanol and steam; ② outlet for gaseous products; ③ inlet for fresh catalyst; ④ discharge for spent catalysts.

Table 1

Operating conditions of the demo-scale DMTO reactor.

Parameters	Value
Temperature, K	773
Gauge pressure at top exit, MPa	0.103
Inflow rate of methanol, kg/h	2032
Inflow rate of steam, kg/h	610
Fresh catalyst inflow rate, kg/h	351
Catalyst inventory in the reaction zone, kg	501

gaseous products are released from the top outlet for further separation and purification. The spent catalysts are discharged from the bottom of the stripper and then transported to the regenerator for restoring the activity. Density and mean diameter of the catalyst particles are 1500 kg/m³ and 97 μm, respectively. Table 1 summarizes the operating conditions.

3. Hydrodynamic models and simulation setup

3.1. Governing equations

The two-fluid model is used to describe the hydrodynamics of gas-solid fluidization, and ANSYS Fluent® version 15 (ANSYS, 2013) is employed as the solver. Relevant governing equations are as follows:

The continuum equation ($q = g, s; p = s, g$) is

$$\frac{\partial}{\partial t}(\varepsilon_q \rho_q) + \nabla \cdot (\varepsilon_q \rho_q \mathbf{u}_q) = \Gamma_{pq} - \Gamma_{qp}, \quad (1)$$

where \mathbf{u}_q is the velocity of phase q and Γ_{pq} is the mass transfer term from the phase p to phase q .

Momentum conservation equations are

$$\begin{aligned} \frac{\partial}{\partial t}(\varepsilon_g \rho_g \mathbf{u}_g) + \nabla \cdot (\varepsilon_g \rho_g \mathbf{u}_g \mathbf{u}_g) = & -\varepsilon_g \nabla p + \nabla \cdot \boldsymbol{\tau}_g + \varepsilon_g \rho_g \mathbf{g} + \mathbf{F}_d \\ & + (\Gamma_{sg} \mathbf{u}_{sg} - \Gamma_{gs} \mathbf{u}_{gs}), \end{aligned} \quad (2)$$

and

$$\begin{aligned} \frac{\partial}{\partial t}(\varepsilon_s \rho_s \mathbf{u}_s) + \nabla \cdot (\varepsilon_s \rho_s \mathbf{u}_s \mathbf{u}_s) = & -\varepsilon_s \nabla p - \nabla p_s + \nabla \cdot \boldsymbol{\tau}_s + \varepsilon_s \rho_s \mathbf{g} \\ & - \mathbf{F}_d + (\Gamma_{gs} \mathbf{u}_{gs} - \Gamma_{sg} \mathbf{u}_{sg}). \end{aligned} \quad (3)$$

The stress tensor is expressed by

$$\boldsymbol{\tau}_q = \varepsilon_q \mu_q [\nabla \mathbf{u}_q + (\nabla \mathbf{u}_q)^T] + \varepsilon_q \left(\lambda_q - \frac{2}{3} \mu_q \right) \nabla \cdot \mathbf{u}_q \mathbf{I}. \quad (4)$$

where the solid pressure p_s , solid viscosity μ_s and solid bulk viscosity λ_s are commonly closed by the Kinetic Theory of Granular Flow (KTGF) (Gidaspow, 1994). \mathbf{u}_{sg} and \mathbf{u}_{gs} are velocities at the gas-solid interface. If $\Gamma_{sg} > 0$, $\mathbf{u}_{sg} = \mathbf{u}_s$, else $\mathbf{u}_{sg} = \mathbf{u}_g$; likewise, If $\Gamma_{gs} > 0$, $\mathbf{u}_{gs} = \mathbf{u}_g$, else $\mathbf{u}_{gs} = \mathbf{u}_s$. The interaction force mainly refers to the drag force in gas-solid fluidization, so \mathbf{F}_d is expressed by $(\mathbf{u}_g - \mathbf{u}_s)\beta$ where β denotes the drag coefficient employing the following expression,

$$\beta = \frac{3}{4} C_{d0} \frac{\rho_s (1 - \varepsilon_s) \varepsilon_s |\mathbf{u}_g - \mathbf{u}_s|}{d_p} \varepsilon_s^{-2.65} H_D. \quad (5)$$

In the above, H_D is the heterogeneity index accounting for the effects of meso-scale structures and defined by β/β_0 (β_0 refers to the drag coefficient for homogeneous fluidization, employing the Wen and Yu correlation) (Wang & Li, 2007). H_D is determined by the EMMS/bubbling model (Hong et al., 2013) in EMMS®2.0 software, and relevant formula can be found in Lu et al. (2017).

Species transport equation ($q = g, s; p = s, g$) is

$$\frac{\partial}{\partial t}(\varepsilon_q \rho_q \mathbf{Y}_{q,i}) + \nabla \cdot (\varepsilon_q \rho_q \mathbf{u}_q \mathbf{Y}_{q,i}) = -\nabla \cdot \mathbf{J}_{q,i} + \varepsilon_q \mathbf{R}_{q,i} + \mathcal{R} + \varepsilon_q \mathbf{S}_{q,i}, \quad (6)$$

where $J_{q,i}$ is diffusive flux of species i in phase q , $R_{q,i}$ the homogeneous reaction rate of species i in phase q , \mathcal{R} the heterogeneous reaction rate and $S_{q,i}$ is the source term accounting for other contributions or reactions. Because relatively constant temperature (around 773 K) is maintained in this DMTO reactor, isothermal simulations are thus employed and the energy conservation equation is not considered.

3.2. Chemical kinetics

In the MTO process, there exist a variety of reaction pathways among reactants, intermediates and different product components (Lesthaeghe et al., 2007). To facilitate the practical application, Ying et al. (2015) proposed a simplified lumped chemical kinetics involving seven parallel reactions between methanol (MeOH denotes methanol in their model) and seven product lumps (i.e. CH₄, C₂H₄, C₃H₆, C₃H₈, C₄, C₅ and coke). In simulation, C₅ and C₄ are represented by C₅H₁₀ and C₄H₈, respectively. The reactant H₂O does not explicitly appear in this parallel reaction network, but its contribution is included in rate laws.

The reaction rate R_i ($i = \text{CH}_4, \text{C}_2\text{H}_4, \text{C}_3\text{H}_6, \text{C}_3\text{H}_8, \text{C}_4, \text{C}_5$ and coke) is written by (unit: g/g_{cat}/s)

$$R_i = v_i k_i \varphi_i C_{\text{MeOH}} M_i. \quad (7)$$

The consumption rate of methanol is given by

$$R_{\text{MeOH}} = \left(-\sum_1^7 v_i k_i \varphi_i \right) C_{\text{MeOH}} M_{\text{MeOH}}. \quad (8)$$

The generation rate of H₂O is

$$R_{\text{H}_2\text{O}} = \left(\sum_1^7 v_i k_i \varphi_i \right) C_{\text{MeOH}} M_{\text{H}_2\text{O}}. \quad (9)$$

where v_i is stoichiometric number ($i = 1, 1/2, 1/3, 1/3, 1/4, 1/5, 1/6$), and k_i (L/g_{cat}/s) is the rate constant, which varies with temperature, as provided in Table 2. C_{MeOH} (mol/L) denotes the concentration of methanol, and M (g/mol) is molecular weight of each lump.

The deactivation function due to the formation of coke is expressed by

$$\varphi_i = \frac{A}{1 + B \exp(D \times (w_c - E))} \exp(-\alpha_i w_c), \quad (10)$$

where $A = 1$, $B = 9$, $D = 2$ and $E = 7.8$, determined by experiment, and α_i is the fitting parameter. The quantities at other temperatures are obtained by linear interpolation and extrapolation. Here, the chemical parameters at 773 K are treated equal to those at 763 K.

3.3. CSTR-estimated initial coke distribution

The mean residence time of catalyst particles in MTO reactor is about 1.43 h, and more than 1.43 h operation is generally required to achieve a relatively steady operation. Our previous study (Lu

et al., 2016) indicated that the simulation of a pilot-scale MTO reactor starting with fresh catalysts could take more than one year to arrive at the steady state on our parallel computers (2CPUs per node, intel-Xeon 2.8G, 10 cores). Therefore, in order to shorten the transitional time from the initial state to the steady state of CFD simulations, we try to establish a reactor model to predict a reasonable coke distribution as the initial distribution of coke in CFD simulations.

For any catalyst particle, the generation of coke deposition on its surface can be written by

$$\frac{dw_c(t)}{dt} = R_{\text{coke}} \cdot 100, \quad (11)$$

where w_c is the coke content of a catalyst particle (g/100g_{cat}) and R_{coke} is the reaction rate of coke. The multiplier of 100 is used to balance the units of both sides of this equation. Substituting Eq. (7) of R_{coke} into Eq. (11), we obtain

$$\frac{dw_c}{dt} = v_{\text{coke}} k_{\text{coke}} \varphi_{\text{coke}} C_{\text{MeOH}} M_{\text{coke}} \cdot 100. \quad (12)$$

On the right hand side (RHS) of Eq. (12), v_{coke} and M_{coke} are constants, and k can be also treated as a constant for isothermal simulations. Thus, only the deactivation function φ and methanol concentration C_{MeOH} vary with position and time.

Letting C_0 represent the constant part of Eq. (12), i.e. $C_0 = v_{\text{coke}} k_{\text{coke}} M_{\text{coke}} \cdot 100$ and substituting Eq. (10) into Eq. (12) yields

$$\frac{1}{A} \frac{1 + B \exp(D \times (w_c - E))}{\exp(-\alpha_i w_c)} dw_c = C_0 C_{\text{MeOH}} dt. \quad (13)$$

Integrating with the limit that at $t = 0$, then $w_c = 0$, we obtain

$$\begin{aligned} & \frac{1}{\alpha_i} (\exp(\alpha_i w_c) - 1) + \frac{B}{\exp(DE)(D + \alpha_i)} (\exp((\alpha_i + D)w_c) - 1) \\ & = AC_0 t \frac{1}{t} \int_0^t C_{\text{MeOH}} dt. \end{aligned} \quad (14)$$

The local methanol concentration at any instant in time is not easily accessible. As a first approximation of a turbulent reactor, $\frac{1}{t} \int_0^t C_{\text{MeOH}} dt$ can be considered equal to the methanol concentration which is averaged over the whole reaction zone (Li et al., 2015), $\overline{C_{\text{MeOH}}}$. Then, Eq. (14) can be rewritten as

$$\begin{aligned} & \frac{1}{\alpha_i} (\exp(\alpha_i w_c) - 1) + \frac{B}{\exp(DE)(D + \alpha_i)} (\exp((\alpha_i + D)w_c) - 1) \\ & = AC_0 t \overline{C_{\text{MeOH}}}. \end{aligned} \quad (15)$$

Consequently, the coke content w_c is a function of the age of catalyst particles and the average methanol concentration, i.e. $w_c = w_c(t, \overline{C_{\text{MeOH}}})$. Because we employ the CSTR model to represent the macroscopic mixing behavior of this DMTO reactor, the age distribution of catalyst particles inside a CSTR (Li et al., 2015) can be expressed by

Table 2
Reaction rate constant k_i and the fitting parameter α_i at different temperatures.

Reaction	Rate constant k_i (L/g _{cat} /s)			α_i		
	723 K	748 K	763 K	723 K	748 K	763 K
1	0.00232	0.00300	0.00501	0.0576	0.0649	0.043
2	0.10030	0.12463	0.15413	0.0914	0.1008	0.0982
3	0.15817	0.16212	0.19234	0.1743	0.1996	0.2017
4	0.03699	0.03467	0.04252	0.3462	0.406	0.4099
5	0.07519	0.07910	0.09094	0.2575	0.2924	0.2929
6	0.05159	0.04895	0.04895	0.3759	0.3495	0.3336
7	0.05436	0.05859	0.07432	0.3817	0.3856	0.3793

$$I(t) = \frac{1}{\tau} e^{-t/\tau}. \quad (16)$$

The average coke content can be related to the age distribution of catalyst particles as

$$\bar{w}_c = \int_0^{\infty} w_c(t, \bar{C}_{\text{MeOH}}) I(t) dt, \quad (17)$$

where \bar{C}_{MeOH} falls in the range ($C_{\text{MeOH,in}}, C_{\text{MeOH,out}}$). The average coke content \bar{w}_c can be also determined by using the molar balance equations of the CSTR (Lu et al., 2016) as follows.

The coke balance is

$$G_s w_{c,in} + I_s R_c = G_s \bar{w}_c. \quad (18)$$

The balance between the reactants and gaseous species is

$$Q_{in} C_{j,in} + \frac{I_s R_j}{M_j} = Q_{out} C_j. \quad (19)$$

The overall concentration of all gaseous species is

$$\sum C_j = \frac{P}{1000RT}. \quad (20)$$

where G_s (g/s) represents the mass flow rates of catalysts through the system, I_s total catalyst inventory (g) and Q (L/s) is the volumetric flow rate of gas phase, respectively. Because the reactions do not greatly change the mean molecular weight of the gas phase, the volumetric inflow rate is approximately equal to the volumetric outflow rate. The constant pressure and temperature are employed, and the subscript j denotes all the gaseous species. In the CSTR model, the concentrations of all the species at the exit are the same as those in the reactor. Therefore, if knowing operating parameters and product distribution at the exit, the average coke content \bar{w}_c can be obtained solving Eqs.(18)–(20), i.e. 7.41 g/100g_{cat}. The distribution of coke content is then calculated in MATLAB by resolving Eqs. (15)–(17) with the input parameter, \bar{w}_c (≈ 7.41 g/100g_{cat}). As illustrated in Fig. 2, the coke content ranges from 0 to 9.2 g/100g_{cat}, and the value near 8 g/100g_{cat} has the biggest probability of presence.

3.4. Simulation settings

In this study, two-dimensional (2D) simulations are employed because the primary quantities from 2D simulations are very close to those from 3D ones (Zhu et al., 2016). The gas distributor is simplified in 2D simulation and the gas inlet is directly set at the upper plane of the distributor, as in the simulation performed by Zhao

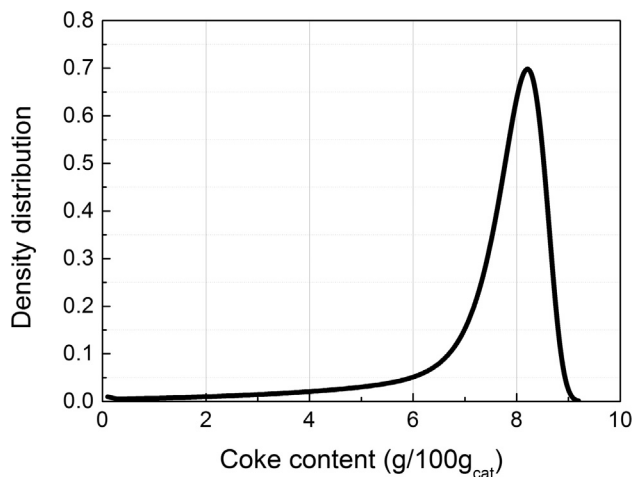


Fig. 2. The distribution of coke content predicted by the CSTR model.

et al. (2013). The solid volume fraction and superficial gas velocity in the reaction zone in 2D simulations are kept the same as in practical operation. The fresh catalysts are fed into the reactor through the inlet labeled ③ in Fig. 1 and the spent catalysts are discharged from the bottom outlet labeled ④. The bottom outlet is also prescribed as the velocity inlet, but the velocity of spent catalysts is against the main gas flow. The top exit for releasing gaseous product is prescribed as pressure outlet. To maintain a constant solid inventory, the solid particles exiting the reactor are monitored and returned to the reactor through the inlet of fresh catalysts. Actually, the solid particles are barely carried out of the reactor because the design of the expanded disengaging bed dramatically reduces the entrainment of particles.

Gambit[®]2.4 is employed to generate the grids. The main reaction zone and the expanded sedimentation bed use the square grids with size of 0.01×0.01 m and 0.015×0.015 m, respectively. Other regions such as the distributor zone employ triangle grids. The total grid number is 84977. The same reactor was simulated by Zhu et al. (2016) where the effects of grid size on 2D simulations were investigated. Because the grid size used in this study is smaller than the finest grid size in Zhu et al. (2016), the grid-dependence test is not repeated here. The time step is 5×10^{-4} s, and the superficial gas velocity is about 1 m/s. Therefore, the Courant number is in the range [0.03–0.05], as recommended by Zhu et al. (2016).

The gas phase is treated as a mixture of nine species (CO_2 , CH_4 , C_2H_4 , C_3H_6 , C_3H_8 , C_4 , C_5 , H_2O and methanol). Note that CO_2 is introduced intentionally as an “inert” gas to improve the numerical stability. The physical properties of these nine species can be obtained from database of NIST (<http://webbook.nist.gov/chemistry>) and Aspen[®]Plus. Due to the strong macroscopic flow in the reactor, the difference in diffusivity of different gaseous species can be almost neglected, so the mass diffusion coefficients for all gas species are set to be equal. Because the coke deposition on the catalysts is closely related to the selectivity of light olefins while does not virtually affect the hydrodynamic behaviors of particles, the catalysts with different coke contents are differentiated only in the species transport. Here, the solid phase is set to have $N+1$ catalyst species with different coke contents (in this study, $N=5, 10, 15$ and 20) where the first solid species refer to the fresh catalysts with the initial mass fraction of zero, and the other N species have their respective coke content. The mass fractions of these N solid species are determined by dividing the coke content in the range [0, 9.2] (shown in Fig. 2) into N equal parts and calculating the area of each interval below the curve. The coke content of each interval is prescribed as the arithmetic mean. The mass variation of all the species is expressed in the form of source terms of species transport equation, therefore the terms \mathbf{R} and \mathcal{R} in Eq. (6) are actually not used. Other settings are listed in Table 3.

4. Results and discussion

4.1. The effect of solid species number

Large species number means higher accuracy but also higher computing demand. Therefore, we first compare four cases with different solid species number (i.e. $N=5, 10, 15$ and 20) and then determine the suitable setting for further discussion.

The variation of solid volume fraction in the main reaction zone with increasing species number, N , is monitored and presented in Fig. 3. At the beginning period, the solids concentration fluctuates differently with varying N . However, after a period of time, i.e. 50 s, the solids concentrations of four cases level off and their averages are close to one another.

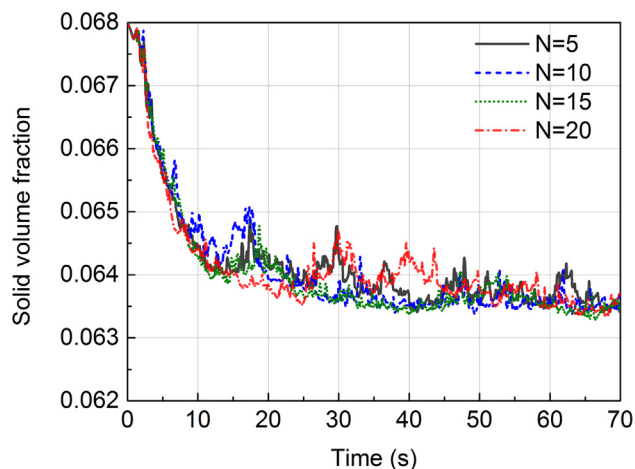
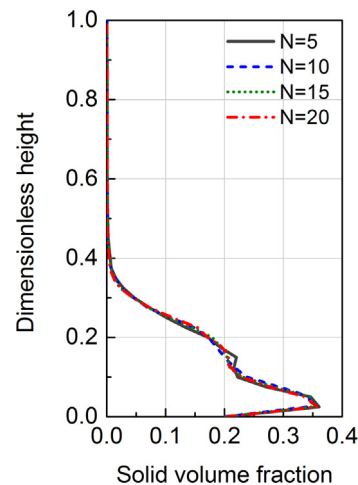
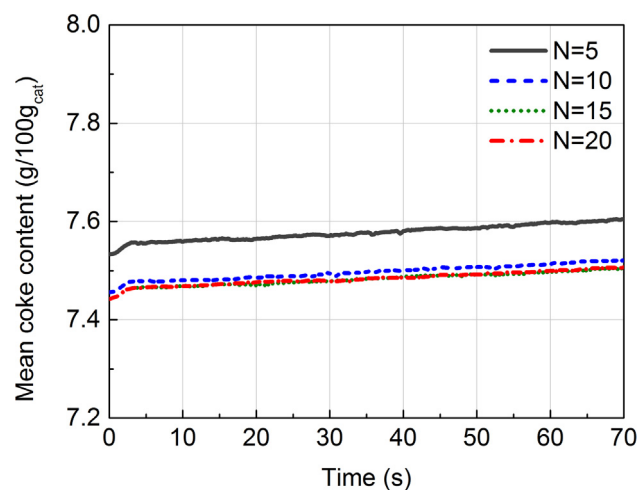
Table 3
CFD simulation settings.

Pressure-velocity Coupling	Phase Coupled SIMPLE
Gradient discretization	Green-Gauss Cell Based
Momentum discretization	Second-order upwind
Volume fraction discretization	QUICK
Wall boundary	No-slip
Granular temperature	Algebraic
Granular viscosity	Gidaspow
Granular bulk viscosity	Lun et al.
Frictional viscosity	Schaeffer
Frictional pressure	Based-ktgf
Angel of internal friction	30.0007
Solid pressure	Lun et al.
Radial distribution	Lun et al.
Restitution coefficient	0.9
Friction packing limit	0.61
Packing limit	0.63
Time step (s)	0.0005
Max iteration of one time step	40

The comparison of mean solids concentration for four cases is illustrated in Fig. 4. Four axial profiles nearly overlap. They show a very dense bottom, especially in the vicinity of the gas distributor and almost no particles above the position of “0.4” are detected. Both Figs. 3 and 4 indicate that considering the distribution of coke content has almost no influence on the prediction in macroscopic hydrodynamics.

As the coke content is closely related to the reaction rate, we investigated the reaction-related quantities in the following. Fig. 5 shows the variation of mean coke contents with time for all four cases. For $N = 5$, the predicted mean coke content is significantly larger than those of the other three cases. The other three cases provide similar results, and the curves of $N = 15$ and $N = 20$ nearly overlap. Fig. 6 presents the instantaneous distribution of mass fraction of methanol. The four cases show different instantaneous distributions of methanol, but all reveal that most of methanol is consumed in the vicinity of the distributor and only a little methanol remains above the height of 1 m. The distributions of time-average mass fraction of methanol for four cases which are provided in the supplementary material, are very similar.

All the simulations were conducted on our parallel computers by employing 24 processes (CPU E5-2692 v2). We compared the run time for all four cases together with the simulation without consideration of coke distribution, as shown in Fig. 7. The first case (dubbed TFM-A) also uses the combination of TFM and the EMMS/bubbling drag model while considers the average coke content for the catalysts, as in our previous study (Lu et al., 2016, 2017).

**Fig. 3.** Solid volume fraction of in the main reaction zone versus time.**Fig. 4.** The axial profiles of mean solids concentration in the reaction zones of four cases (The y origin denotes the position of the upper plane of the distributor).**Fig. 5.** Variation of mean coke content in the main reaction zone with time.

Compared with our previous simulation approach (TFM-A in Fig. 7), all the other cases considering the coke distribution spend more time to achieve the pseudo-steady state. For a run simulating the realistic process for 1 s, the run time increases with N . Based on these results, we selected $N = 15$ for further study.

4.2. Distribution of coke content

Fig. 8 presents the distribution of coke content at the initial state and after an elapse of 70 s. Because the coke generation rate is extremely low, the evolution of 70 s results in only a minor change in the coke distribution. Although these results cannot directly indicate that the initial distribution obtained from the CSTR model is close to the pseudo-steady coke distribution, we will check the relevant reaction quantities in the following to prove the rationality of this coke distribution.

It is found from Fig. 8 that catalyst particles with lower coke content occupy a relatively low percentage but their impact on the overall reaction rate seems not negligible because increase in the coke content will suppress the reaction. Thus, when the temperature and the methanol concentration are kept constant, only the coke content plays a role in reaction rate. The contribution of each coke interval to the overall reaction rate on the basis of the Faver average is presented in Fig. 9. It is evident that the catalyst

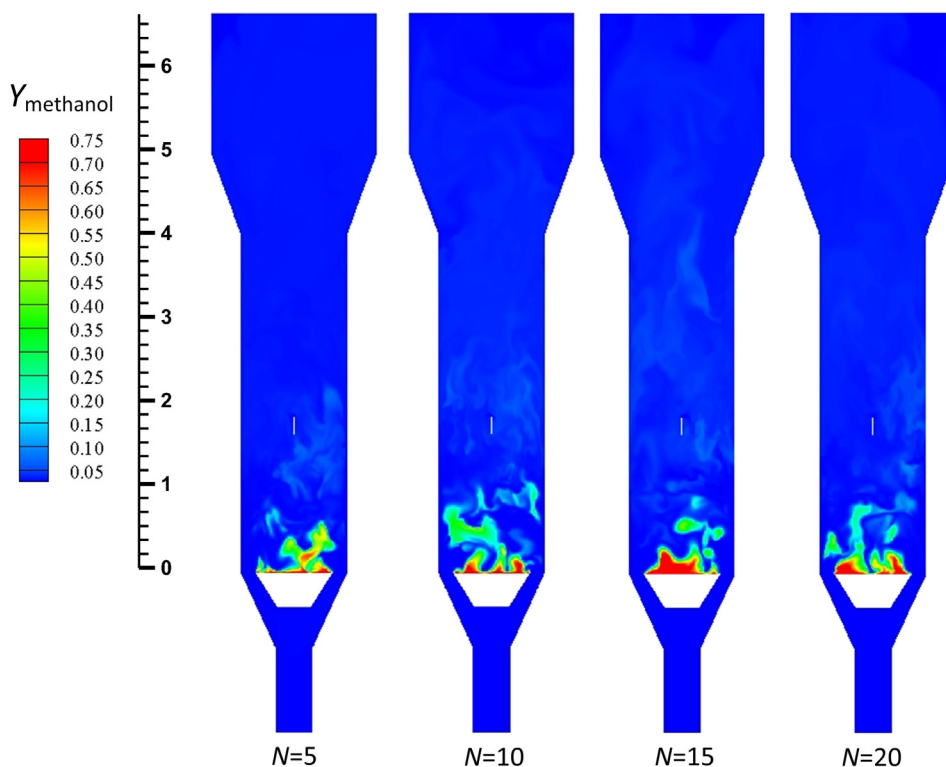


Fig. 6. Instantaneous distribution of mass fraction of methanol on the axial cross section.

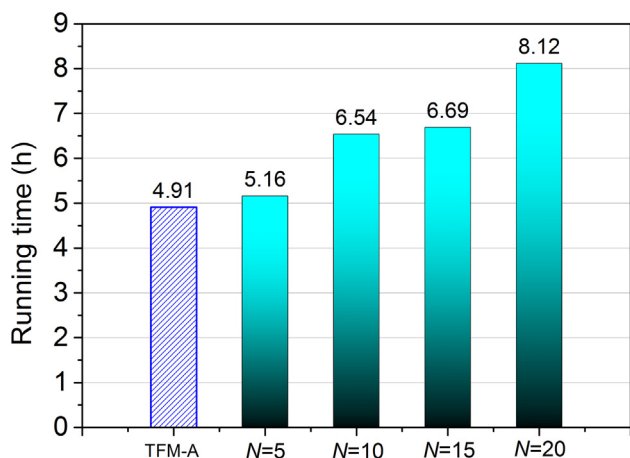


Fig. 7. The required time for simulating a realistic process for 1 s.

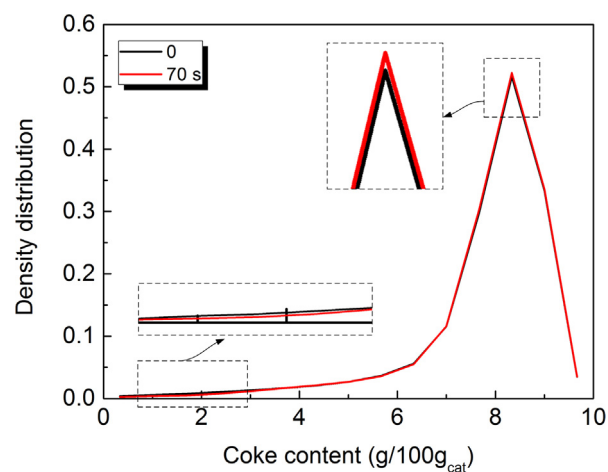


Fig. 8. Coke content density distribution.

particles with lower coke content have marked influence on the overall reaction rate. This also demonstrates that considering the distribution of coke content rather than using average coke content is much reasonable to predict the reaction quantities.

4.3. Gaseous products

Fig. 10 presents the instantaneous distributions of the reactant, methanol and the primary product, ethylene (the figure of time-average value is provided in the [supplementary material](#)). For the reactant (methanol), compared with the left hand side (LHS) case without considering the coke distribution, the RHS case reveals more consumption of methanol in the vicinity of the gas distributor. The methanol conversions for two cases are then calculated, i.e. 94.72% for LHS case and 97.23% for RHS case. With considering the coke distribution, the simulation predicts higher methanol

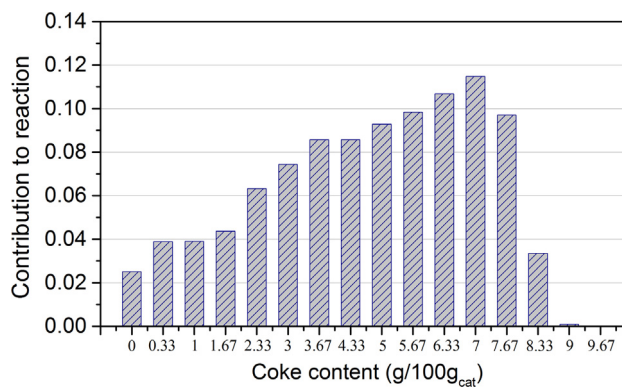


Fig. 9. The contribution of each interval to the overall reaction rate.

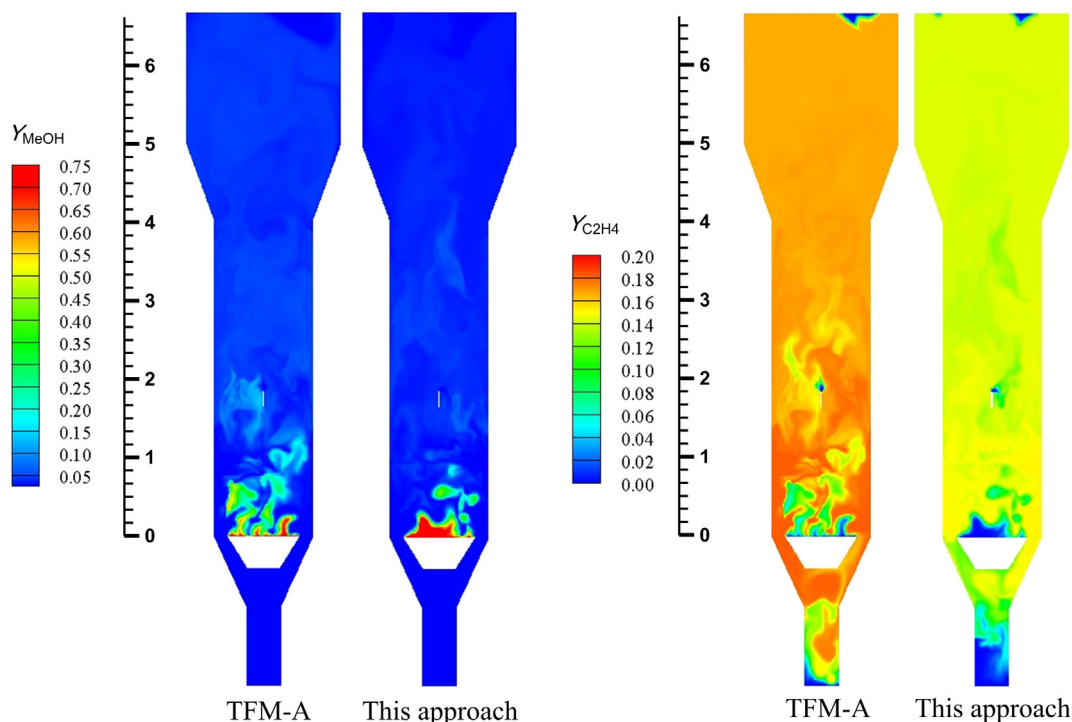


Fig. 10. Instantaneous distribution of mass fraction of methanol and ethylene on the axial cross section (TFM-A: without consideration of coke distribution; this approach: considering coke distribution with the number of solid species $N = 15$).

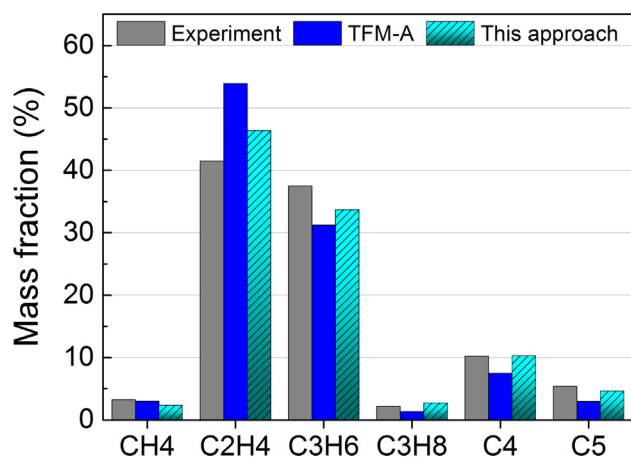


Fig. 11. Mass fraction of gaseous product obtained from CFD simulation and experiment (the mass fractions are normalized after removing H_2O , methanol and CO_2).

conversion, closer to the experimental value of 99.97%. The present discrepancy is probably attributed to the fact that the 2D geometry reduces the mixing to some extent. For the primary product (ethylene), the case considering the coke distribution predicts lower ethylene concentration. This is due to the fact that the catalysts with lower coke deposition allow more gaseous products diffusing out of the catalysts and hence lowering the selectivity of ethylene.

The mass fractions of all the gaseous products provided by experiment and simulations are illustrated in Fig. 11. If we use the previous TFM approach without consideration of coke distribution, the ethylene is highly over-predicted and the propylene is under-predicted. When differentiating the catalyst particles with different coke contents, the predictions in gaseous products are greatly improved. More quantitative comparisons are given in Table 4. It can be seen that the sum of C_2H_4 and C_3H_6 predicted by this approach is approximately 80%, very close to the experimental value of 79%. The ratio of C_2H_4 to C_3H_6 is reduced from 1.73 to 1.38 by using this approach. The present deviation from the experiment ($C_2H_4/C_3H_6 \approx 1.1$) needs further research on the chemical kinetics.

Table 4

Comparison of simulation predictions and experimental data (the mass fractions are normalized after removing H_2O , methanol and CO_2).

Parameters	Exp.	TFM-A	Error (%)	This approach	Error (%)
Y_{CH_4} (%)	3.22	3.02	6.21	2.34	27.28
$Y_{C_2H_4}$ (%)	41.47	53.93	30.05	46.36	11.80
$Y_{C_3H_6}$ (%)	37.48	31.21	16.73	33.67	10.16
$Y_{C_3H_8}$ (%)	2.21	1.36	38.46	2.71	22.51
Y_{C_4} (%)	10.24	7.50	26.76	10.29	0.53
Y_{C_5} (%)	5.37	2.99	44.32	4.62	13.93
$Y_{(C_2H_4+C_3H_6)}$ (%)	78.95	85.14	7.84	80.03	1.37
C_2H_4/C_3H_6	1.11	1.73	55.86	1.38	24.05
\bar{w}_c (g/100g _{cat})	7.70	7.44	3.38	7.50	2.60
η_{MeOH} (%)	99.97	94.42	5.76	97.23	2.74

5. Conclusions and future work

A CSTR model considering the residence time was established to predict both the mean value and distribution of coke content. Then, the solid phase was considered to consist of a series of species to differentiate the catalyst particles with different coke contents under the TFM framework. A 2D demo-scale MTO reactor was simulated and solid species number was chosen to be 15 for further study. Compared with our previous simulation without consideration of coke distribution, this approach incorporating the coke distribution requires 36% more computational time and shows almost no influence on predictions in hydrodynamic behaviors, but the reaction quantities such as methanol conversion, mass fractions of gaseous products and the selectivity of light olefins, are better predicted. Discrepancies in predictions of ethylene and propylene are probably attributed to the use of the chemical kinetics based on the experiments over a micro-scale fluidized bed.

Acknowledgement

This work is financially supported by the National Natural Science Foundation of China under Grant nos. 21576263 and 21625605, China's State Key Laboratory of Multiphase Complex Systems under Grant no. MPCs-2017-A-03, and the Youth Innovation Promotion Association of Chinese Academy of Sciences under Grant no. 2015033.

Appendix A. Supplementary material

Supplementary data associated with this article can be found, in the online version, at <https://doi.org/10.1016/j.ces.2018.05.056>.

References

- Alwahabi, S.M., Froment, G.F., 2004. Conceptual reactor design for the methanol-to-olefins process on SAPO-34. *Ind. Eng. Chem. Res.* 43 (17), 5112–5122.
- Amghizar, I., Vandewalle, L.A., Van Geem, K.M., Marin, G.B., 2017. New trends in olefin. *Prod. Eng.* 3 (2), 171–178.
- ANSYS, Inc., 2013. ANSYS Fluent Theory Guide (release 15.0). <<http://www.ansys.com>>.
- Bos, A.N.R., Tromp, P.J.J., Akse, H.N., 1995. Conversion of methanol to lower olefins. Kinetic modeling, reactor simulation, and selection. *Ind. Eng. Chem. Res.* 34 (11), 3808–3816.
- Chang, J., Zhang, K., Chen, H., Yang, Y., Zhang, L., 2013. CFD modelling of the hydrodynamics and kinetic reactions in a fluidised-bed MTO reactor. *Chem. Eng. Res. Des.* 91 (12), 2355–2368.
- Chen, J.Q., Bozzano, A., Glover, B., Fuglerud, T., Kvisle, S., 2005. Recent advancements in ethylene and propylene production using the UOP/Hydro MTO process. *Catal. Today* 106 (1), 103–107.
- Gidaspow, D., 1994. *Multiphase Flow and Fluidization: Continuum and Kinetic Theory Descriptions*. Academic Press, Boston.
- Hong, K., Shi, Z., Wang, W., Li, J., 2013. A structure-dependent multi-fluid model (SFM) for heterogeneous gas–solid flow. *Chem. Eng. Sci.* 99, 191–202.
- Kaarsholm, M., Rafii, B., Joensen, F., Cenni, R., Chaouki, J., Patience, G.S., 2010. Kinetic modeling of methanol-to-olefin reaction over ZSM-5 in fluid bed. *Ind. Eng. Chem. Res.* 49 (1), 29–38.
- Keil, F.J., 1999. Methanol-to-hydrocarbons: process technology. *Microporous Mesoporous Mater.* 29 (1), 49–66.
- Kraft, S., Kirnbauer, F., Hofbauer, H., 2017. Influence of drag laws on pressure and bed material recirculation rate in a cold flow model of an 8MW dual fluidized bed system by means of CPFD. *Particuology*. <https://doi.org/10.1016/j.partic.2017.04.009>.
- Lesthaeghe, D., Van Speybroeck, V., Marin, G.B., Waroquier, M., 2007. The rise and fall of direct mechanisms in methanol-to-olefin catalysis: an overview of theoretical contributions. *Ind. Eng. Chem. Res.* 46 (26), 8832–8838.
- Li, H., Ye, M., Liu, Z., 2016. A multi-region model for reaction–diffusion process within a porous catalyst pellet. *Chem. Eng. Sci.* 147, 1–12.
- Li, J., Kwauk, M., 2003. Exploring complex systems in chemical engineering—the multi-scale methodology. *Chem. Eng. Sci.* 58 (3–6), 521–535.
- Li, X., Ying, L., Cheng, Y., Wang, L., 2015. Simulation of multi-fluidized-bed in series for methanol to olefins (in Chinese). *CIESC J.* 66 (8), 3041–3049.
- Lu, B., Luo, H., Li, H., Wang, W., Ye, M., Liu, Z., Li, J., 2016. Speeding up CFD simulation of fluidized bed reactor for MTO by coupling CRE model. *Chem. Eng. Sci.* 143, 341–350.
- Lu, B., Zhang, J., Luo, H., Wang, W., Li, H., Ye, M., Liu, Z., Li, J., 2017. Numerical simulation of scale-up effects of methanol-to-olefins fluidized bed reactors. *Chem. Eng. Sci.* 171, 244–255.
- Luna, C.M.R., Carrocci, L.R., Arce, G.L.A.F., Ávila, I., 2017. A comparative assessment of empirical and lattice Boltzmann method-based drag models for simulation of gas–solid flow hydrodynamics in a bubbling fluidized bed. *Particuology* 33, 129–137.
- Luo, H., Lu, B., Zhang, J., Wu, H., Wang, W., 2017. A grid-independent EMMS/bubbling drag model for bubbling and turbulent fluidization. *Chem. Eng. J.* 326, 47–57.
- Schoenfelder, H., Kruse, M., Werther, J., 1996. Two-dimensional model for circulating fluidized-bed reactors. *AIChE J.* 42 (7), 1875–1888.
- Soundararajan, S., Dalai, A.K., Berruti, F., 2001. Modeling of methanol to olefins (MTO) process in a circulating fluidized bed reactor. *Fuel* 80 (8), 1187–1197.
- Stroh, A., Alobaid, F., Hasenzahl, M.T., Hilz, J., Ströhle, J., Epple, B., 2016. Comparison of three different CFD methods for dense fluidized beds and validation by a cold flow experiment. *Particuology* 29, 34–47.
- Tian, P., Wei, Y., Ye, M., Liu, Z., 2015. Methanol to Olefins (MTO): from Fundamentals to Commercialization. *ACS Catal.* 5 (3), 1922–1938.
- Wang, W., Li, J., 2007. Simulation of gas–solid two-phase flow by a multi-scale CFD approach—extension of the EMMS model to the sub-grid level. *Chem. Eng. Sci.* 62 (1–2), 208–231.
- Yang, N., Wang, W., Ge, W., Li, J., 2003. Choosing structure-dependent drag coefficient in modeling gas–solid two-phase flow. *China Particuol.* 1 (1), 38–41.
- Ye, M., Li, H., Zhao, Y., Zhang, T., Liu, Z., 2015. Chapter five – MTO processes development: the key of mesoscale studies. *Adv. Chem. Eng.* 47, 279–335.
- Ying, L., Yuan, X., Ye, M., Cheng, Y., Li, X., Liu, Z., 2015. A seven lumped kinetic model for industrial catalyst in DMTO process. *Chem. Eng. Res. Des.* 100, 179–191.
- Yuan, X., Li, H., Ye, M., Liu, Z., 2017. Comparative study of MTO kinetics over SAPO-34 catalyst in fixed and fluidized bed reactors. *Chem. Eng. J.* 329, 35–44.
- Zhao, Y., Li, H., Ye, M., Liu, Z., 2013. 3D Numerical simulation of a large scale MTO fluidized bed Reactor. *Ind. Eng. Chem. Res.* 52, 11354–11364.
- Zhu, L.T., Ye, M., Luo, Z.H., 2016. Application of filtered model for reacting gas–solid flows and optimization in a large-scale methanol-to-olefin fluidized-bed reactor. *Ind. Eng. Chem. Res.* 55 (46), 11887–11899.
- Zhuang, Y.Q., Chen, X.M., Luo, Z.H., Xiao, J., 2014. CFD–DEM modeling of gas–solid flow and catalytic MTO reaction in a fluidized bed reactor. *Comput. Chem. Eng.* 60, 1–16.